



# HHS Public Access

Author manuscript

*Nat Cell Biol.* Author manuscript; available in PMC 2017 August 27.

Published in final edited form as:

*Nat Cell Biol.* 2017 April ; 19(4): 391–398. doi:10.1038/ncb3481.

## Tubulin acetylation protects long-lived microtubules against mechanical aging

Didier Portran<sup>1</sup>, Laura Schaedel<sup>2</sup>, Zhenjie Xu<sup>1</sup>, Manuel Théry<sup>2,3</sup>, and Maxence V. Nachury<sup>1,\*</sup>

<sup>1</sup>Department of Molecular and Cellular Physiology, Stanford University School of Medicine, CA 94305, USA

<sup>2</sup>Laboratoire de Physiologie Cellulaire et Végétale, Institut de Recherche en Technologie et Science pour le Vivant, UMR5168, CEA/INRA/CNRS/UGA, 38054 Grenoble, France

<sup>3</sup>Unité de Thérapie Cellulaire, Hôpital Saint Louis, Institut Universitaire d'Hématologie, UMRS1160, INSERM/AP-HP/Université Paris Diderot, 75010 Paris, France

### INTRODUCTORY PARAGRAPH

Long-lived microtubules endow the eukaryotic cell with long-range transport abilities. While long-lived microtubules are acetylated on lysine 40 of  $\alpha$ -tubulin ( $\alpha$ K40), acetylation takes place after stabilization<sup>1</sup> and does not protect against depolymerization<sup>2</sup>. Instead,  $\alpha$ K40 acetylation has been proposed to mechanically stabilize microtubules<sup>3</sup>. Yet how modification of  $\alpha$ K40, a residue exposed to the microtubule lumen and inaccessible from MAPs and motors<sup>1,4</sup>, could affect microtubule mechanics remains an open question. Here we develop FRET-based assays that report on the lateral interactions between protofilaments and find that  $\alpha$ K40 acetylation directly weakens inter-protofilament interactions. Congruently,  $\alpha$ K40 acetylation affects two processes largely governed by inter-protofilament interactions, reducing the nucleation frequency and accelerating the shrinkage rate. Most relevant to the biological function of acetylation, microfluidics manipulations demonstrate that  $\alpha$ K40 acetylation enhances flexibility and confers resilience against repeated mechanical stresses. Thus, unlike deacetylated microtubules that accumulate damages when subjected to repeated stresses, long-lived microtubules are protected from mechanical aging through their acquisition of  $\alpha$ K40 acetylation. Thus, unlike other tubulin post-translational modifications that act through MAPs, motors and severing enzymes, intraluminal acetylation directly tunes the compliance and resilience of microtubules.

### Keywords

Microtubule;  $\alpha$ TAT1;  $\alpha$ K40 acetylation; persistence length; flexibility; protofilaments lateral interaction

Users may view, print, copy, and download text and data-mine the content in such documents, for the purposes of academic research, subject always to the full Conditions of use: [http://www.nature.com/authors/editorial\\_policies/license.html#terms](http://www.nature.com/authors/editorial_policies/license.html#terms)

\*Correspondence and requests for materials should be addressed to M.V.N. (nachury@gmail.com).

### AUTHOR CONTRIBUTIONS

Z.X. was involved in the initial conceptualization of the project. M.V.N. and M.T. designed the study. D.P. developed and conducted the enzymatic modifications of tubulin, self-assembly assays and electron microscopy. L.S. performed the measurement and analysis of microtubule persistence length and material fatigue. M.V.N. and D.P. wrote the manuscript with input from all authors.

The authors declare no competing financial interests.

## MAIN TEXT

Microtubules with hour-long half-lives found in cytoplasm, cilia and axons must preserve their structural integrity in the face of ubiquitous mechanical stresses to maintain tracks for intracellular transport. Paradoxically, while microtubules assembled *in vitro* have millimeter-long persistence lengths and are as stiff as Plexiglas<sup>5,6</sup>, long-lived microtubules in cells are frequently highly buckled due to the compressive loads generated by microtubule-based molecular motors and actomyosin contractility<sup>7,8</sup>. How long-lived microtubules acquire mechanical stability is not known.

$\alpha$ K40 acetylation has recently emerged as a candidate for the mechanical stabilization of microtubules because nematodes mutant for the  $\alpha$ K40 acetyltransferase  $\alpha$ TAT1/MEC-17 experience profound microtubule defects including protofilament number variability, fragmentation and lattice opening<sup>9-11</sup>. To characterize the biochemical consequences of  $\alpha$ K40 acetylation, we enzymatically modified brain tubulin (30% acetylated) then removed the enzymes to generate pure preparations of acetylated (>96%) and deacetylated (<1% acetylated) tubulin (Fig. 1a and Supplementary Fig. 1a,b,c). Absolute levels of acetylation were determined by comparison with ciliary tubulin, a standard known to be 100% acetylated<sup>12</sup>. Surprisingly, acetylated tubulin self-assembled much slower than deacetylated tubulin while brain tubulin showed intermediate kinetics (Fig. 1b). The effects of TAT1 and SIRT2 on microtubule self-assembly were fully reversible (Supplementary Fig. 1d-f), confirming that it is acetylation *per se* and not the enzymes themselves that impinge on the kinetics of polymerization. Self-assembly of tubulin is kinetically limited by nucleation and reaches an apparent steady-state once polymerization and depolymerization balance one another. Consistent with the increased lag phase of self-assembly for acetylated tubulin, acetylation decreased the spontaneous nucleation rate by 2.7-fold (Fig. 1c, Supplementary Fig. 2a,b). Further supporting the conclusion that acetylation reduces microtubule nucleation, addition of pre-formed microtubule seeds to acetylated tubulin rapidly accelerated self-assembly and the steady-state levels of microtubules became nearly identical between deacetylated and acetylated samples once seeds had been supplied (Fig. 1d). The pronounced effects of acetylation on nucleation of pure tubulin demonstrate that acetylation directly regulates a molecular interaction within the microtubule lattice without the need for a molecular intermediate. We thus sought to pinpoint the specific molecular interactions within the lattice that are altered by acetylation.

Microtubule nucleation is thought to entail the assembly of short protofilaments through longitudinal (i.e. head-to-tail) interactions between  $\alpha/\beta$ -tubulin dimers, the formation of small sheets through parallel inter-protofilament interactions; lateral and longitudinal extension then lead to sheet closure into a 13- to 15-protofilament tube<sup>13</sup> (Fig. 1e). Similarly, microtubule polymerization and depolymerization are governed by longitudinal and lateral interactions but in subtly different ways. Microtubule depolymerization entails the outward curving of protofilaments imparted by the GDP-bound conformation of tubulin and peeling of protofilaments away from one other<sup>14</sup>. The relative energetics of outward protofilament bending and lateral cohesion between neighboring protofilaments is thus expected to govern depolymerization<sup>15</sup>. Meanwhile, in the elongating microtubule, a GTP cap is predicted to

lock protofilaments into a straight conformation and the rate of subunit addition is most closely influenced by longitudinal interactions (see model in Fig. 1e). Consequently, the strengthening of lateral interprotofilament interactions is expected to slow depolymerization while minimally affecting growth rates<sup>16</sup>. Measurements of single microtubule dynamics showed no detectable difference in the growth rate of deacetylated and acetylated microtubules (Fig. 1f and Supplementary Fig. 2b). Strikingly, acetylated microtubules depolymerized threefold faster than deacetylated microtubules (Fig. 1f and Supplementary Fig. 2b). These data are consistent with lateral, but not longitudinal, interactions being reduced by acetylation.

To more directly assess the dynamics of longitudinal and lateral interactions between tubulin dimers, we developed a FRET-based assay that monitors the self-assembly events preceding nucleation (Fig. 2a). When experiments were conducted in the presence of GTP but below the critical concentration for microtubule self-assembly, no microtubules were observed (Supplementary Fig. 2c) yet FRET between tubulin dimers was readily detected, indicative of self-assembly without overt polymerization (Fig. 2b). This assay reports on relevant interactions between tubulin dimers as self-assembly was undetectable in the presence of GDP (Fig. 2f and Supplementary Fig. 2d). Consistent with the finding that deacetylation accelerates a step that precedes nucleation, the pre-nucleation self-assembly rate of deacetylated tubulin was six times faster than that of acetylated tubulin (Fig. 2b,f). Even in the presence of taxol, a strong promoter of microtubule nucleation, self-assembly of tubulin was accelerated four times by deacetylation (Fig. 2c,f). Furthermore, deacetylated tubulin still self-assembled faster than acetylated tubulin in presence of the slowly hydrolysable GTP analogues GTP $\gamma$ S or GMPCPP (Fig. 2d–f), indicating that acetylation does not exert its effects through a modulation of GTP hydrolysis. Congruently, the rate of GTP hydrolysis during microtubule polymerization was unaffected by the degree of  $\alpha$ K40 acetylation (Supplementary Fig. 2e). In this context, it is notable that the catastrophe frequency was unaffected by acetylation, indicating that the stochastic loss of the GTP cap is not influenced by acetylation (Supplementary Fig. 2b).

To determine whether acetylation alters the geometry and strength of longitudinal interactions between tubulin dimers, we assessed protofilament curvature and length after protofilament assembly at 4°C<sup>17</sup> (Fig. 2g and Supplementary Fig. 2f). In agreement with structural studies of  $\alpha$ - $\beta$  end-to-end contacts<sup>18,19</sup>, GTP $\gamma$ S, GTP, GMPCPP and GTP/taxol protofilaments became progressively straighter in individually assembled protofilaments (Fig. 2h,i and Supplementary Fig. 3a–f). Importantly, no significant differences in length or radius were detected between deacetylated and acetylated protofilaments regardless of the nucleotide status of tubulin (Fig. 2h,i and Supplementary Fig. 3e,f). Collectively, our analysis of protofilament shape suggests that  $\alpha$ K40 acetylation does not modify longitudinal interactions and leaves inter-protofilament interactions as the most likely affected parameter in self-assembly. We note that protofilaments are longer in the presence of GTP $\gamma$ S (Supplementary Fig. 3e), and the resulting increase in the number of laterally interacting subunits may partially mask the inhibition of self-assembly by acetylation (Fig. 2d,f). Meanwhile, by straightening protofilaments (Fig. 2i, Supplementary Fig. 3c and Ref. <sup>17,20</sup>), taxol facilitates interprotofilament interactions and mitigates the effect of acetylation on self-assembly (Fig. 2c,f). The acetylation-dependent decrease of self-assembly rates is most

greatly attenuated by GMPCPP (Fig. 2e,f), likely because GMPCPP both lengthens and straightens protofilaments (Supplementary Fig. 3d–f) thus combining the apparent effects of taxol and GTP $\gamma$ S on self-assembly.

To directly test the hypothesis that  $\alpha$ K40 acetylation weakens lateral interactions, we developed a biophysical FRET-based assay that reports on the strength of inter-protofilament interactions (Fig. 3a). Following the observation that tubulin assembles into protofilaments in the presence of taxol and GTP at 4°C (Supplementary Fig. 3c and Ref. <sup>21</sup>) and that at least 85% of the tubulin oligomerizes into protofilaments under these conditions (Supplementary Fig. 3g), we generated labelled protofilaments preparations in GDP-containing buffer (Supplementary Fig. 3h,i). In the absence of GTP, raising the temperature did not lead to microtubule polymerization (see Fig. 4a,b). However, incubation of the protofilaments in the presence of GDP at 32°C led to an increase in FRET signal indicative of protofilament- protofilament interactions (Fig. 3b,e). Because free tubulin incubated under the same conditions did not produce detectable FRET signal (Fig. 3c,e) and free tubulin mixed with protofilaments only yielded a modest FRET signal (Fig. 3d,e), we conclude that longitudinal interactions do not significantly contribute to the FRET signal and that the FRET assay reports on inter-protofilament interactions without signal contamination from the free tubulin remaining in the protofilament preparation. Strikingly, acetylation decreased protofilament self-association five-fold (Fig. 3b,e). Pelleting assays confirmed that a greater mass of oligomers was generated by assembly of deacetylated protofilaments than with acetylated protofilaments (Fig. 3f and Supplementary Fig. 4b). Since neither protofilament length nor curvature were affected by the acetylation status at  $\alpha$ K40 (Supplementary Fig. 3i), these results indicate that tubulin acetylation directly reduces either  $\alpha$ - $\alpha$  or  $\beta$ - $\beta$  lateral contacts.

Extending the results from the FRET assay, negative stain EM showed that deacetylated protofilaments assembled into large sheets while acetylated protofilaments remained for the most part isolated with only rare instances of two to three protofilaments associating with one another (Fig. 4a–c and Supplementary Fig. 5a,b). Importantly, analysis of diffraction patterns<sup>22</sup> demonstrated that the incubation of protofilaments produced sheets organized in parallel arrays, similarly to the organization of the microtubule lattice (Fig. 4d,e). The diffraction pattern of sheets produced by the protofilament assay was asymmetrical, as was the pattern generated by sheet-like structures at the open ends of microtubules (Fig. 4d,e). Meanwhile the diffraction pattern of antiparallel zinc sheets was instead symmetrical (Fig. 4f). A weakening of lateral  $\alpha$ - $\alpha$  or  $\beta$ - $\beta$  interactions by  $\alpha$ K40 acetylation thus provides a unifying explanation for the reduced nucleation rate, accelerated shrinkage and decreased inter-protofilament association of acetylated tubulin (Fig. 1e). Interestingly, while acetylated and deacetylated microtubules assembled from pure tubulin normally have the same number of protofilaments, acetylation enriches 13-protofilament microtubules and depletes 14-protofilament microtubules when microtubules are incubated in the presence of kinesin<sup>23</sup>. One interpretation is that, because of slight geometrical differences, lateral interactions in 14-protofilament microtubules are more reliant on  $\alpha$ K40 than in 13-protofilament microtubules. Consequently, acetylation of  $\alpha$ K40 may destabilize 14-protofilament microtubules against the torque imposed by the power stroke of kinesin. In agreement with biophysical evidence that lateral contacts between protofilaments are extremely

tenuous<sup>24–26</sup>, a 3.5 Å structure of microtubules finds  $\alpha$ - $\alpha$  and  $\beta$ - $\beta$  contacts consisting of a single aromatic residue captured by a pocket on the lateral neighbor<sup>19</sup>. Since  $\alpha$ K40 buttresses one of the two loops that form side-to-side contacts<sup>27</sup>, it has been proposed that an electrostatic bond involving  $\alpha$ K40 alters the strength of  $\alpha$ - $\alpha$  interactions<sup>9,23</sup>. This hypothesis has however eluded structural investigations as the nine amino acids flanking  $\alpha$ K40 remain the last unsolved part of the  $\alpha/\beta$ -tubulin core<sup>19</sup>, even in a 4.2 Å structure of microtubules assembled from non-acetylated recombinant tubulin<sup>28</sup>. Together, these data suggest that the  $\alpha$ K40 loop is flexible and that the lateral contact whose strength is reduced by  $\alpha$ K40 acetylation is itself dynamic.

As microtubule acetylation takes place post-assembly in cells and acetylated microtubules are protected from depolymerization<sup>3</sup>, we rationalized the reduction of inter-protofilament interactions by  $\alpha$ K40 acetylation in the biological context of microtubule mechanics. By distributing material away from the central axis, the tubular architecture dramatically increases flexural rigidity compared to a filamentous organization<sup>29</sup>. At the same time, a longitudinal opening will convert the tube into a highly flexible planar sheet. Similarly, inter-protofilament sliding within the lattice has been proposed to facilitate microtubule bending<sup>25,30,31</sup>. We predicted that the weakening of lateral interactions by  $\alpha$ K40 acetylation may decrease flexural rigidity. Microtubule mechanics were studied using our recently described system<sup>32</sup> where dynamic microtubules grow from stabilized microtubule seeds grafted onto micropatterns and are subjected to an orthogonal flow measured *in situ* with fiduciary beads (Fig. 5a). Consistent with our hypothesis, acetylation greatly increased microtubule flexibility (Fig. 5b, Supplementary Fig. 5c,d). Furthermore, similar to microtubules assembled from brain tubulin<sup>32</sup>, the flexural rigidity of deacetylated microtubules decreased with each consecutive bending cycle, evidencing the material fatigue of deacetylated microtubules (Fig. 5c,d, Supplementary Fig. 5c–f, Supplementary Video 1). In stark contrast, the flexural rigidity of acetylated microtubules remained unchanged in face of repeated bending cycles, thus demonstrating that acetylation suppresses material fatigue and limits the aging of long-lived microtubules.

We propose that the weakening of lateral interactions by  $\alpha$ K40 acetylation prevents pre-existing lattice defects from spreading into large areas of damage under repeated stress<sup>33,34</sup> (Fig. 5e).  $\alpha$ K40 acetylation is thus predicted to make long-lived microtubules less susceptible to breakage in contexts where they are subjected to repetitive cycles of bending. The acquisition of microtubule resilience through  $\alpha$ K40 acetylation is best exemplified in the touch receptor neurons that run along the longitudinal axis of nematode. The microtubules in these neurons are bent by the sinusoidal movements of the animal and ablation of the  $\alpha$ K40 acetyltransferase leads to axonal microtubule breakages<sup>9,10</sup> that can be rescued by paralyzing the animal<sup>11</sup>. Cardiomyocytes represent a particularly dramatic example of repeated microtubule stresses as the compressive forces generated by sarcomere shortening are resisted by microtubules that buckle under axial load<sup>35</sup>. Tubulin detyrosination was found to be important in anchoring stable microtubules to the sarcomere<sup>35</sup> and, while there is no direct link between detyrosination and acetylation of tubulin, it will be of interest to test whether acetylation protects cardiomyocyte microtubules from breakage resulting from repetitive buckling.

Finally, recent studies have found that TAT1 can enter the microtubule either through the ends or through defects along the lattice<sup>36–38</sup>. Furthermore, it is conceivable that bending produces transient and local breathing events that enable TAT1 entry and local  $\alpha$ K40 acetylation<sup>37</sup>. Local acetylation near lattice defects and areas subjected to stress may therefore increase resilience in areas most prone to mechanical breakage.

## ONLINE METHODS

### Tubulin purification and labelling

No cell lines were used in this study. Bovine brain tubulin was purified as previously described<sup>39</sup>. Briefly, tubulin was purified from pig brain extract by two cycles of polymerization/depolymerization in high-molarity PIPES buffer. Brain, acetylated and deacetylated tubulin were labeled with either rhodamine-NHS (Thermo), NHS-atto-488 (Sigma), NHS-LC-LC-biotin (EZ-link, Thermo) or NHS-DyLight 650 (Thermo) as described<sup>40</sup>. The labeling of acetylated and of deacetylated tubulin stocks were conducted side by side for each fluorophore. The labelling stoichiometries were nearly identical for acetylated and deacetylated tubulin stocks and were approximately 1 fluorophore per dimer for Atto 488-labeled tubulin, 0.6 for rhodamine-labeled tubulin and 0.25 for DyLight 650-labeled tubulin.

### Protein expression and purification

Proteins were expressed in Escherichia coli Rosetta2 after induction with 0.2 mM IPTG at 16 °C overnight. TAT1[2-236] was purified using Glutathione Sepharose 4B and eluted into 2XT (40 mM Tris, pH 7.4, 400 mM NaCl, and 5 mM DTT) by overnight cleavage with PreScission protease (GE Healthcare). His-tagged SIRT2 was expressed in bacteria (plasmid is gift from Eric Verdin) and purified using Ni-NTA beads and eluted into 2XT (40 mM Tris, pH 7.4, 400 mM NaCl, and 5 mM  $\beta$ -mercaptoethanol) supplemented with 100 mM imidazole. All proteins were aliquoted into single-use aliquots after addition of 5% glycerol.

### Enzymatic modification of tubulin

Tubulin was acetylated or deacetylated by adding TAT1 [2-236] construct or SIRT2 into ADE buffer (40 mM PIPES pH 6.9, 0.8 mM EGTA, 0.4 mM MgSO<sub>4</sub>, 4.0 M Glycerol). 100  $\mu$ M of acetyl Co-enzyme A (Sigma) was added for TAT1-mediated acetylation, and 1 mM NAD<sup>+</sup> (Sigma) was added for SIRT2-mediated deacetylation. The reactions were incubated for 1h at 4°C and 1h at 24°C. Microtubules were then allowed to fully polymerize for 1h at 30°C and subsequently submitted to two cycles of polymerization/depolymerization in High Molarity PIPES buffer<sup>39</sup>. One cycles of polymerization/depolymerization was repeated until no trace of enzymes was detected by Coomassie staining. The final tubulin preparations were aliquoted in BRB80, flash frozen and stored in liquid nitrogen.

### Absolute quantitation of $\alpha$ -tubulin K40 acetylation

The levels of acetylation at  $\alpha$ K40 were measured by quantitative immunoblotting using a Li-Cor infrared laser scanner (Odyssey), ensuring that measurements were in the linear range of the instrument. For immunoblotting, 1 ng of tubulin was resolved by SDS-PAGE, transferred onto a 0.45  $\mu$ M PVDF membrane, probed with the 6-11-B1 anti- $\alpha$ K40 acetylated tubulin

monoclonal antibody (Sigma T6793) and Dylight 800-conjugated anti-mouse IgG (Thermo 35521) and the membrane was scanned at 800 nm. For Coomassie staining, 1  $\mu$ g of tubulin was resolved by SDS-PAGE and the gel scanned at 700 nm. To measure absolute levels of acetylation, we included a *Tetrahymena* ciliary tubulin, a standard previously demonstrated to be a 100% acetylated by Edman sequencing<sup>12</sup>.

### Turbidity assay

Tubulin assembly was monitored by following the increase of turbidity as the absorbance at 350 nm (SmartSpec 3000 spectrophotometer, Biorad). Prior to the experiment, tubulin solutions were centrifuged for 5 min at 227,000  $\times g_{ave}$  (80,000 rpm, TLA100.2) to remove oligomers and aggregated tubulin. 50  $\mu$ M of modified tubulin was diluted in BRB80 with 1 mM GTP and 5% glycerol and 5 mM DTT in a quartz cuvette and incubated at 37°C for the assembly measurement. Tubulin disassembly was triggered by placing the cuvette in iced cold water. Time points were taken every 5 min for 1h for the assembly phase and then every 2 min for 15 min for the disassembly phase.

### GTPase assay

Prior to the experiment, tubulin solutions were centrifuged for 5 min at 227,000  $\times g_{ave}$  (80,000 rpm, TLA100.2) to remove oligomers and aggregated tubulin. 50  $\mu$ l reactions were assembled in BRB80 with 10  $\mu$ M tubulin, 0.5 mM GTP, 0.5 mM DTT and 5% Glycerol. Spontaneous GTP hydrolysis was controlled with a reaction composed of 0.5 mM GTP, 0.5 mM DTT and 5% Glycerol in BRB80. Reactions were incubated either at 4°C or at 37°C or at 37°C in presence of 1  $\mu$ M of GMPCPP-stabilized microtubule seeds (free GMPCPP was removed from the microtubule seeds by centrifugation and resuspension in BRB80). After 2.5 h, the reactions were stopped by addition of 5  $\mu$ l of 50% TCA in BRB80 with 0.5 mM GTP and incubated for 2 min on ice. The samples were rapidly centrifuged to remove aggregates and 30  $\mu$ l samples were transferred to a clear-bottom 96-well plate (Sigma, Nunc MicroWell) and combined with 70  $\mu$ l of Cytophos reagent (BK054, Cytoskeleton) to measure the amounts of inorganic phosphate. The reactions were incubated for 10 min at 20°C after addition of Cytophos and the absorbance at 650 nm was recorded using a Polarstar Omega multimodes microplate reader. A phosphate standard curve was established, ranging from 0.1 to 2 nmol.

### Microtubule nucleation assay

0.5, 5 or 10  $\mu$ M free tubulin (unlabeled and rhodamine-labeled tubulin stocks were mixed so that 10% of the tubulin was rhodamine-labeled) was incubated at 37°C in BRB80, 1 mM GTP and 5 % glycerol. Microtubules were fixed with 0.5% glutaraldehyde in BRB80 after 5 of 15 min and then centrifuged through a glycerol cushion on a coverslip. The microtubules were imaged using a standard epifluorescence microscope equipped with a 60x oil immersion (Zeiss). The microtubules were counted using imageJ.

### Imaging of microtubule dynamics by TIRF microscopy

Total internal reflection microscopy imaging of microtubule dynamics *in vitro* was conducted as follow: Microtubule seeds were polymerized with 0.5 mM GMPCPP from a 10

$\mu\text{M}$  mixture of rhodamine-labelled, biotin-labelled, and unlabeled tubulin dimers in a 4:2:1 ratio at  $37^\circ\text{C}$  for 30 min. Glass coverslips were cleaned by bath sonication for 15 min successively in 1 M NaOH, 2% Hellmanex III (Hellma), acetone and ethanol (96%). The clean coverslips were silanized in a solution of trichloroethylene with 0.2% dimethyldichlorosilane for 2h at room temperature and then washed 3 times in methanol and 3 times in MilliQ water. Fully sealed flow cells were mounted onto a TIRF-equipped DeltaVision workstation (Applied Precision, Issaquah, WA) and imaged with a PlanApo  $60\times/1.40\text{NA}$  objective (Olympus, Central Valley, PA), warmed to  $37^\circ\text{C}$  by a temperature-controlled environmental chamber. Dynamic microtubules were elongated from the stabilized microtubule seeds by the addition of  $7\ \mu\text{M}$  tubulin (mixture of unlabeled and Atto 488-labeled tubulin at 19:1 ratio) with 1 mM GTP. Dynamic microtubules were imaged by TIRF using a 488nm laser for excitation (QLM, Deltavision). Microtubule seeds were imaged in the Cy3 channel. Dual-emission data were collected at 2 s intervals for 15 min.

### Imaging of protofilaments by negative stain EM

Formvar carbon coated grids (Electron Microscopy Sciences) were exposed for 45 s to deep UV and then coated with poly-L-Lysine for 1 min to increase protein adsorption. Protofilament samples were absorbed to grids for 30 s and then negatively stained with 1.5% uranyl acetate for 25 s. For the visualization of protofilaments lateral association into sheets, the taxol-stabilized protofilaments in BRB80 with 1 mM GDP were incubated at  $37^\circ\text{C}$  directly onto the formvar carbon coated grids. Protofilaments and protofilaments sheets were visualized using a JEOL 1400 electron microscope at 120 kV at a final magnification of 25,000 x. Protofilament length and radius were manually measured using imageJ by drawing a polyline on the protofilaments and fitting a circle from the polyline (using Fit Circle, ImageJ). The width of the tubulin sheets was measured manually using ImageJ and was reported as a number of protofilaments using a width of 4 nm for protofilament. To confirm that the tubulin sheets represent pre-assembled protofilaments associated in parallel arrays, we compared the diffraction patterns<sup>22</sup> of sheets to that of open sheets at the plus end of taxol stabilized microtubules (parallel protofilament organization) and to tubulin sheets assembled in presence of zinc (antiparallel protofilament organization) using the Fourier shape analysis of imageJ.

### Pre-nucleation self-assembly assay

A step-by-step protocol can be found on Protocol Exchange<sup>41</sup>. Prior to the assay, free tubulin solutions were centrifuged for 5 min at  $227,000 \times g_{ave}$  (80,000 rpm, TLA100.2) to remove oligomers and aggregated tubulin. Rhodamine- and DyLight 650-labeled tubulin stocks were mixed with unlabeled tubulin so that 10% of the tubulin was rhodamine-labeled and 10% DyLight 650-labeled. The reactions were composed of 0.5 to  $5\ \mu\text{M}$  free tubulin in BRB80, nucleotides (1 mM GTP, GDP, GTP $\gamma$ S, or 0.5 mM GMPCPP or 1mM GTP with 0.5 to  $5\ \mu\text{M}$  taxol). The reactions were then transferred to a thermostated cuvette within a Fluoromax-3 fluorimeter (Horiba) pre-equilibrated at  $32^\circ\text{C}$ . The emitter fluorophore was excited at 561 nm and the acceptor fluorescence was recorded at 702 nm with a 4 nm bandwidth at 15s capture interval, 10s measurement time, and for a total acquisition time of 30 min. For each time point, the background fluorescence measured at time zero was subtracted from the fluorescent signal. The oligomerization rate was calculated by



measuring the slope of the progress curve before steady-state was reached. If steady-state was not reached within the time frame of the experiment, then the slope of the entire curve was used to calculate the rate.

Imaging of the reaction products was conducted similarly to the nucleation assay. A rhodamine-labeled tubulin stock was mixed with unlabeled tubulin so that 10% of the tubulin was rhodamine-labeled. A mixture of unlabeled and rhodamine-labeled tubulin at 9:1 molar ratio was incubated for 30 min, reactions were fixed with 0.5% glutaraldehyde in BRB80 for 5 min and centrifuged through a glycerol cushion onto coverslips.

### Protofilament preparation and pelleting assays

Protofilament assembly was conducted by incubating 0.5  $\mu\text{M}$  tubulin in BRB80 with 1 mM GTP, 0.5  $\mu\text{M}$  taxol (Sigma T-7402) and 5% glycerol for 30 min at 4°C. The protofilaments were then dialyzed in BRB80 containing 0.5  $\mu\text{M}$  taxol for 1h at 4°C using a D-tube Dialyser Mini (MWCO 6–8 kDa, Novagen) and 1 mM GDP was added after dialysis. To estimate the amount of protofilaments, solutions were centrifuged at 424,000  $\times g_{ave}$  (100,000 rpm, TLA100 rotor) for 1h at 4°C. To estimate the amount of protofilament sheets, reactions were centrifuged at 86,000  $\times g_{ave}$  (45,000 rpm, TLA100.3 rotor) for 30 min at 37°C. The pellet and supernatant fractions were collected, and tubulin amounts in each fraction were determined by SDS-PAGE, Coomassie staining and gel scanning at 700 nm (Licor, Odyssey). As a control, free tubulin in presence of GDP and taxol was centrifuged under the same conditions.

### Protofilament assembly and association assay

A step-by-step protocol can be found on Protocol Exchange<sup>41</sup>. A rhodamine-labeled tubulin stock was mixed with unlabeled tubulin so that 10% of the tubulin was rhodamine-labeled. In a parallel reaction, Dylight 650-labeled tubulin stocks was mixed with unlabeled tubulin so that 10% of the tubulin was Dylight 650-labeled. Protofilament assembly was conducted by incubating 0.5  $\mu\text{M}$  tubulin in BRB80 with 1 mM GTP, 0.5  $\mu\text{M}$  taxol (Sigma T-7402) and 5% glycerol for 30 min at 4°C. In order to prevent protofilament elongation during the FRET assay, the free GTP remaining in the protofilament preparations was removed by dialysis into BRB80 containing 0.5  $\mu\text{M}$  taxol for 1h at 4°C using a D-tube Dialyser Mini (MWCO 6–8 kDa, Novagen). After dialysis, 1 mM GDP was added to the protofilament preparations to further prevent microtubule assembly. Pelleting at 424,000  $\times g_{ave}$  (100,000 rpm, TLA100 rotor) for 1h demonstrated that at least 85 % of the tubulin was present in oligomer form after the protofilaments assembly procedure (Supplementary Fig. 3g). Protofilament morphology was characterized by negative stain EM. The morphologies of acetylated and deacetylated protofilaments were nearly identical (see Supplementary Fig. 3a–d). After addition of GDP, the rhodamine- and DyLight 650-labeled protofilament solutions were mixed together at a 1:1 ratio transferred to a thermostated cuvette within a Fluoromax-3 fluorimeter (Horiba) pre-equilibrated at 32 °C to initiate the protofilaments association assay. The emitter fluorophore was excited at 561 nm and the acceptor fluorescence was recorded at 702 nm with a 4 nm bandwidth at 15s capture interval, 10s measurement time, and for a total acquisition time of 30 min. For each time point, the background fluorescence measured at time zero was subtracted from the fluorescent signal.

The protofilament association rate was calculated by measuring the slope of the progress curve before steady state was reached. To control for the signal obtained from the free tubulin dimers in solution, 0.5  $\mu\text{M}$  of protofilaments (assembled from 0.5  $\mu\text{M}$  solution in which 10% of the tubulin is rhodamine-labeled) were mixed with 0.5  $\mu\text{M}$  free tubulin (5% of the tubulin is Dylight 650-labeled) to approximate the free tubulin left in solution after protofilament assembly (Fig. 3d).

### Microtubules flexibility measurement

Microtubule bending experiment were performed as previously described<sup>32</sup> using microtubule micropatterning in a microfluidic chip. Briefly, biotinylated GMPCPP-stabilized microtubule seeds were attached to micropatterns and microtubules were allowed to elongate from the seeds by the addition of 14  $\mu\text{M}$  of free tubulin dimers in presence of 1 mM GTP. The flow inside the microfluidic chip was controlled using a microfluidic pump (MDCS-4C, fluigent). For repeated bending experiments, the flow was turned on for 10 s and then turned off for 10 s, repeating this cycle up to seven times. Fiduciary fluorescent beads, present in solution in the same focal plane as the microtubules, allowed for the *in situ* measurement of the flow speed imposed on the microtubules lattice. Microtubules were visualized using an objective-based azimuthal ilas2 TIRF microscope (Nikon Eclipse Ti, modified by Roper Scientific) and an Evolve 512 camera (Photometrics). The microscope stage was kept at 37 °C by means of a warm stage controller (LINKAM MC60). Excitation was achieved using lasers with wavelengths of 491 and 561 nm (Optical Insights). Microtubule flexibility was calculated using a previously described methodology<sup>32</sup>.

### Code availability

The computer code used for analysis of microtubule curvature and calculation of persistence length was previously described<sup>32</sup> and is available from the corresponding author on request.

### Data availability

All data supporting the conclusions are available from the corresponding author on reasonable request.

### Statistics and reproducibility

Statistical analyses were performed with Kaleidagraph (Synergy software) and RealStat (Excel, Microsoft). Statistical significance was assessed by a two-tailed *p*-value calculated using either a Student's *t*-test or a non-parametric (Mann-Whitney) analysis as indicated in the legend. The experiments presented in figure 3d, 3f, in supplementary figure 1e and 1f were performed once. All other experiments were independently repeated at least twice. For each experiment the number of samples that were analyzed as well as the number of repeated independent experiments are indicated in the figure legend. All samples were included in the analysis. Experiments where microtubule dynamics were substantially different from the usual parameters were excluded. This criterion was pre-established. No statistical method was used to predetermine sample size. The experiments were not randomized. The investigators were not blinded to allocation during experiments and outcome assessment.

## Supplementary Material

Refer to Web version on PubMed Central for supplementary material.

## Acknowledgments

This work was supported by HFSP Grant RGY0088/2012 to M.V.N. and M.T., ERC grant 310472 to M.T. and a Stanford School of Medicine Dean's Postdoctoral Fellowship to D.P. We thank B.K. Kobilka for the use of his fluorimeter, J. Al-Bassam for advice and assistance on imaging of microtubule dynamics, E. Nogales for comments on the manuscript and E. Verdin for the SIRT2 expression construct. The Jeol JEM1400 TEM was funded by NIH grant 1S10RR02678001 to the Stanford Microscopy Facility.

## References

1. Janke C, Bulinski JC. Post-translational regulation of the microtubule cytoskeleton: mechanisms and functions. *Nat Rev Mol Cell Biol.* 2011; 12:773–786. [PubMed: 22086369]
2. Palazzo A, Ackerman B, Gundersen GG. Cell biology: Tubulin acetylation and cell motility. *Nature.* 2003; 421:230. [PubMed: 12529632]
3. Garnham CP, Roll-Mecak A. The chemical complexity of cellular microtubules: tubulin post-translational modification enzymes and their roles in tuning microtubule functions. *Cytoskeleton.* 2012; 69:442–463. [PubMed: 22422711]
4. Soppina V, Herbstman JF, Skiniotis G, Verhey KJ. Luminal localization of  $\alpha$ -tubulin K40 acetylation by cryo-EM analysis of fab-labeled microtubules. *PLoS ONE.* 2012; 7:e48204. [PubMed: 23110214]
5. Gittes F, Mickey B, Nettleton J, Howard J. Flexural rigidity of microtubules and actin filaments measured from thermal fluctuations in shape. *J Cell Biol.* 1993; 120:923–934. [PubMed: 8432732]
6. Hawkins T, Mirigian M, Selcuk Yasar M, Ross JL. Mechanics of microtubules. *J Biomech.* 2010; 43:23–30. [PubMed: 19815217]
7. Brangwynne CP, et al. Microtubules can bear enhanced compressive loads in living cells because of lateral reinforcement. *J Cell Biol.* 2006; 173:733–741. [PubMed: 16754957]
8. Bicek AD, et al. Anterograde microtubule transport drives microtubule bending in LLC-PK1 epithelial cells. *Mol Biol Cell.* 2009; 20:2943–2953. [PubMed: 19403700]
9. Cueva JG, Hsin J, Huang KC, Goodman MB. Posttranslational acetylation of  $\alpha$ -tubulin constrains protofilament number in native microtubules. *Curr Biol.* 2012; 22:1066–1074. [PubMed: 22658592]
10. Topalidou I, et al. Genetically separable functions of the MEC-17 tubulin acetyltransferase affect microtubule organization. *Curr Biol.* 2012; 22:1057–1065. [PubMed: 22658602]
11. Neumann B, Hilliard MA. Loss of MEC-17 leads to microtubule instability and axonal degeneration. *Cell Rep.* 2014; 6:93–103. [PubMed: 24373971]
12. LeDizet M, Piperno G. Identification of an acetylation site of *Chlamydomonas* alpha-tubulin. *Proc Natl Acad Sci USA.* 1987; 84:5720–5724. [PubMed: 2441392]
13. Voter WA, Erickson HP. The kinetics of microtubule assembly. Evidence for a two-stage nucleation mechanism. *J Biol Chem.* 1984; 259:10430–10438. [PubMed: 6469971]
14. Mandelkow EM, Mandelkow E, Milligan RA. Microtubule dynamics and microtubule caps: a time-resolved cryo-electron microscopy study. *J Cell Biol.* 1991; 114:977–991. [PubMed: 1874792]
15. Molodtsov MI, et al. A molecular-mechanical model of the microtubule. *Biophys J.* 2005; 88:3167–3179. [PubMed: 15722432]
16. VanBuren V, Odde DJ, Cassimeris L. Estimates of lateral and longitudinal bond energies within the microtubule lattice. *Proc Natl Acad Sci USA.* 2002; 99:6035–6040. [PubMed: 11983898]
17. Elie-Caille C, et al. Straight GDP-tubulin protofilaments form in the presence of taxol. *Curr Biol.* 2007; 17:1765–1770. [PubMed: 17919908]
18. Alushin GM, et al. High-resolution microtubule structures reveal the structural transitions in  $\alpha\beta$ -tubulin upon GTP hydrolysis. *Cell.* 2014; 157:1117–1129. [PubMed: 24855948]
19. Zhang R, Alushin GM, Brown A, Nogales E. Mechanistic Origin of Microtubule Dynamic Instability and Its Modulation by EB Proteins. *Cell.* 2015; 162:849–859. [PubMed: 26234155]

20. Wang HW, Long S, Finley KR, Nogales E. Assembly of GMPCPP-bound tubulin into helical ribbons and tubes and effect of colchicine. *Cell Cycle*. 2005; 4:1157–1160. [PubMed: 16123589]
21. Schiff PB, Fant J, Horwitz SB. Promotion of microtubule assembly in vitro by taxol. *Nature*. 1979; 277:665–667. [PubMed: 423966]
22. Shibata K, et al. A single protofilament is sufficient to support unidirectional walking of dynein and kinesin. *PLoS ONE*. 2012; 7:e42990. [PubMed: 22900078]
23. Howes SC, et al. Effects of tubulin acetylation and tubulin acetyltransferase binding on microtubule structure. *Mol Biol Cell*. 2014; 25:257–266. [PubMed: 24227885]
24. Tuszyński JA, Luchko T, Portet S, Dixon JM. Anisotropic elastic properties of microtubules. *Eur Phys J E Soft Matter*. 2005; 17:29–35. [PubMed: 15864724]
25. Pampaloni F, et al. Thermal fluctuations of grafted microtubules provide evidence of a length-dependent persistence length. *Proc Natl Acad Sci USA*. 2006; 103:10248–10253. [PubMed: 16801537]
26. Wu Z, Nogales E, Xing J. Comparative studies of microtubule mechanics with two competing models suggest functional roles of alternative tubulin lateral interactions. *Biophys J*. 2012; 102:2687–2696. [PubMed: 22735518]
27. Nogales E, Whittaker M, Milligan RA, Downing KH. High-resolution model of the microtubule. *Cell*. 1999; 96:79–88. [PubMed: 9989499]
28. Vemu A, et al. Structure and Dynamics of Single-isoform Recombinant Neuronal Human Tubulin. *Journal of Biological Chemistry*. 2016; 291:12907–12915. [PubMed: 27129203]
29. Howard, J. *Mechanics of Motor Proteins and the Cytoskeleton*. Sinauer Associates Incorporated; 2001.
30. Needleman DJ, et al. Radial compression of microtubules and the mechanism of action of taxol and associated proteins. *Biophys J*. 2005; 89:3410–3423. [PubMed: 16100275]
31. Sui H, Sui H, Downing KH, Downing KH. Structural basis of interprotofilament interaction and lateral deformation of microtubules. *Structure*. 2010; 18:1022–1031. [PubMed: 20696402]
32. Schaedel L, et al. Microtubules self-repair in response to mechanical stress. *Nat Mater*. 2015; 14:1156–1163. [PubMed: 26343914]
33. Chrétien D, Metoz F, Verde F, Karsenti E, Wade RH. Lattice defects in microtubules: protofilament numbers vary within individual microtubules. *J Cell Biol*. 1992; 117:1031–1040. [PubMed: 1577866]
34. Schaap IAT, de Pablo PJ, Schmidt CF. Resolving the molecular structure of microtubules under physiological conditions with scanning force microscopy. *Eur Biophys J*. 2004; 33:462–467. [PubMed: 14762705]
35. Robison P, et al. Detyrosinated microtubules buckle and bear load in contracting cardiomyocytes. *Science*. 2016; 352:aaf0659–aaf0659. [PubMed: 27102488]
36. Szyk A, et al. Molecular basis for age-dependent microtubule acetylation by tubulin acetyltransferase. *Cell*. 2014; 157:1405–1415. [PubMed: 24906155]
37. Coombes C, et al. Mechanism of microtubule lumen entry for the  $\alpha$ -tubulin acetyltransferase enzyme  $\alpha$ TAT1. *Proc Natl Acad Sci U S A*. 2016; doi: 10.1073/pnas.1605397113
38. Ly N, et al.  $\alpha$ TAT1 controls longitudinal spreading of acetylation marks from open microtubules extremities. *Sci Rep*. 2016; 6:35624. [PubMed: 27752143]
39. Castoldi M, Popov AV. Purification of brain tubulin through two cycles of polymerization-depolymerization in a high-molarity buffer. *Protein Expr Purif*. 2003; 32:83–88. [PubMed: 14680943]
40. Hyman A, et al. Preparation of modified tubulins. *Meth Enzymol*. 1991; 196:478–485. [PubMed: 2034137]
41. Portran D, Nachury MV. Measurement of tubulin oligomers self-assembly by FRET. *Protocol Exchange*. 2017; doi: 10.1038/protex.2017.008

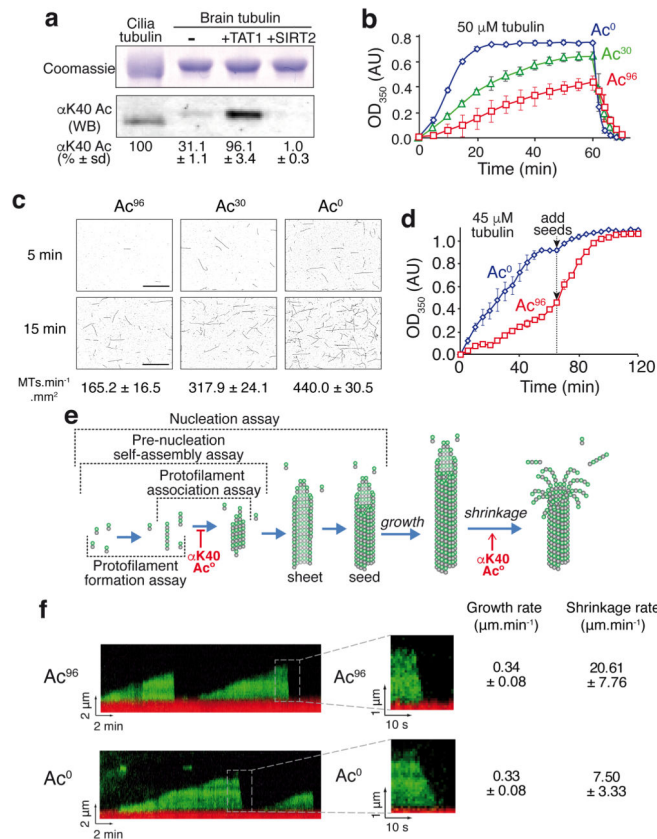


**Figure 1. αK40 acetylation impairs microtubule nucleation and accelerates depolymerization**

**a**, Acetylated (Ac<sup>96</sup>) and deacetylated (Ac<sup>0</sup>) tubulin preparations were produced by treating purified brain tubulin (Ac<sup>30</sup>) with the acetyltransferase TAT1 or the tubulin deacetylase SIRT2 as detailed in Supplementary Fig. 1a. Samples were resolved on SDS-PAGE and Coomassie-stained (top) or immunoblotted for αK40 acetylation (bottom). Axonemal preparations from *Tetrahymena* cilia provide a 100% acetylation calibrator. The measured levels of αK40 acetylation are shown below (mean of n=3 tubulin preparations ± SD). Unprocessed original scans of blots are shown in Supplementary Fig. 1c. **b**, Polymer formation was monitored by following the turbidity, or absorbance at 350 nm, of solutions containing 50 μM tubulin incubated at 37°C. Error bars represent the standard errors of the mean (SEM), n=3 independent experiments for Ac<sup>0</sup>, Ac<sup>30</sup> and Ac<sup>96</sup> tubulin. **c**, Fluorescence images of microtubules nucleated from 10 μM tubulin solutions incubated at 37°C and fixed at 5 and 15 min (images are representative of 3 independent experiments). The mean rate of microtubule nucleation (± SEM) from n=3 independent experiments is shown below each image. Scale bar: 10 μm. **d**, Polymer formation was monitored as in **b**, except that starting tubulin concentration was 45 μM and that 5 μM GMPCPP-stabilized microtubule seeds were added after 70 min. Error bars: SEM, n=3 independent experiments. **e**, Diagram outlining microtubule nucleation and dynamics. The various assays used in this study are outlined and the effects of tubulin acetylation discovered in this study are shown. **f**, Kymographs of dynamic Ac<sup>96</sup> and Ac<sup>0</sup> microtubules imaged by TIRF microscopy (representative of 3 independent experiments). In red are the GMPCPP stabilized microtubule seeds and in green

the dynamic microtubules elongating from the seed. Insets show depolymerizing microtubules at higher magnification. The rates of growth and shrinkage are shown on the right,  $n = 117$  Ac<sup>96</sup> microtubules and  $n = 156$  Ac<sup>0</sup> microtubules (pooled from  $n = 3$  independent experiments, data are mean  $\pm$  SD). Source data for 1b and 1d can be found in Supplementary Table 1.

Author Manuscript

Author Manuscript

Author Manuscript

Author Manuscript

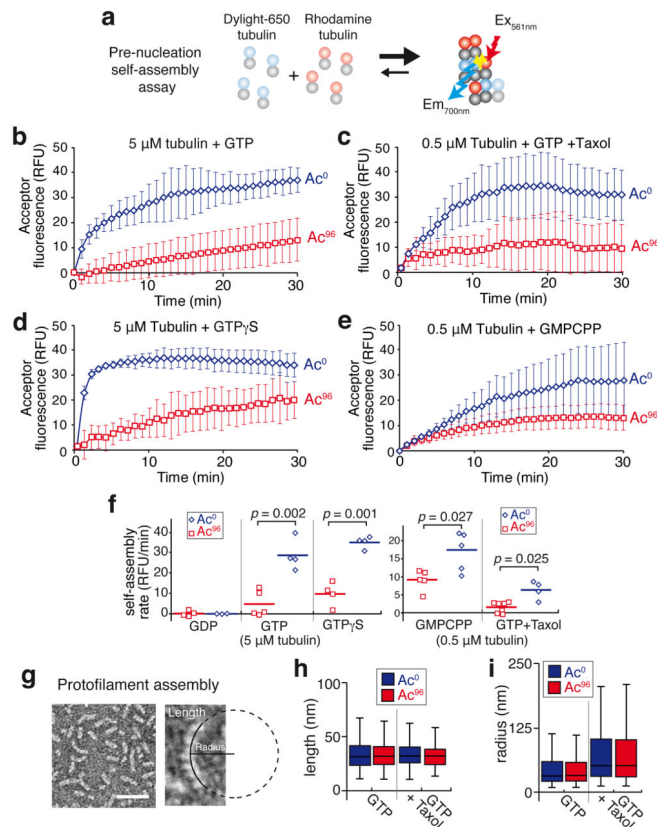


**Figure 2. Tubulin acetylation affects tubulin self-assembly**

**a**, Diagram of the FRET-based pre-nucleation self-assembly assay. **b–e**, Tubulin self-assembly assayed by inter-dimer FRET. A solution of free tubulin below the critical concentration for nucleation in which 10% bears a DyLight 650 label and 10% a rhodamine-label was incubated at 37°C and self-assembly was followed in a spectrofluorimeter by exciting rhodamine at 561 nm and measuring DyLight 650 emission at 700 nm. Data points are mean  $\pm$  SEM, **b**, 5  $\mu$ M tubulin was mixed with 1 mM GTP.  $n=5$  for  $Ac^{96}$  and  $n=4$  for  $Ac^0$  tubulin. **c**, 0.5  $\mu$ M tubulin was mixed with 1 mM GTP + 0.5  $\mu$ M taxol.  $n=7$  for  $Ac^{96}$  and  $n=4$  for  $Ac^0$  tubulin. **d**, 5  $\mu$ M tubulin was mixed with 1 mM GTP $\gamma$ S.  $n=4$  for both  $Ac^{96}$  and  $Ac^0$  tubulin. **e**, 0.5  $\mu$ M tubulin was mixed with 0.5 mM GMPCPP.  $n=5$  for both  $Ac^{96}$  and  $Ac^0$  tubulin.  $n$  values represent the number of independent experiments. **f**, Dot plot of the pre-nucleation self-assembly rates for  $Ac^{96}$  and  $Ac^0$  tubulin. The experiment was done using 5  $\mu$ M of free tubulin with 1 mM GDP, 1 mM GTP or 1 mM GTP $\gamma$ S, or 0.5  $\mu$ M of free tubulin with 1 mM GTP + 0.5  $\mu$ M taxol or 0.5 mM GMPCPP. The bar denotes the mean. The  $p$ -values were calculated using a two-tailed unpaired Student's  $t$ -test. **g**, Taxol-stabilized protofilaments observed by negative stain electron microscopy. The length of each protofilament was measured and a circle was fitted onto the protofilament to measure the radius (images representative of 2 independent experiments). **h,i**, Box plots of the length (**h**) and radius (**i**) of the  $Ac^0$  (blue boxes) and  $Ac^{96}$  (red boxes) protofilaments assembled in the presence of GTP or GTP+taxol. For the GTP condition:  $n=612$   $Ac^0$  protofilaments and  $n=513$   $Ac^{96}$  protofilaments, for the GTP+taxol condition:  $n=542$   $Ac^0$  protofilaments and  $n=536$   $Ac^{96}$  protofilaments (pooled from 2 independent experiments). A Mann-Whitney test

was used to compare Ac<sup>0</sup> and Ac<sup>96</sup> protofilaments populations in each condition. No significant differences were observed between Ac<sup>0</sup> and Ac<sup>96</sup> protofilaments in length ( $p=0.74$  for GTP and  $p=0.07$  for GTP+taxol) or radius ( $p=0.64$  for GTP and  $p=0.94$  for GTP+taxol). The box represents the 25<sup>th</sup>-75<sup>th</sup> percentile, whiskers indicate 1.5 times the range and the bar in the middle is the median.



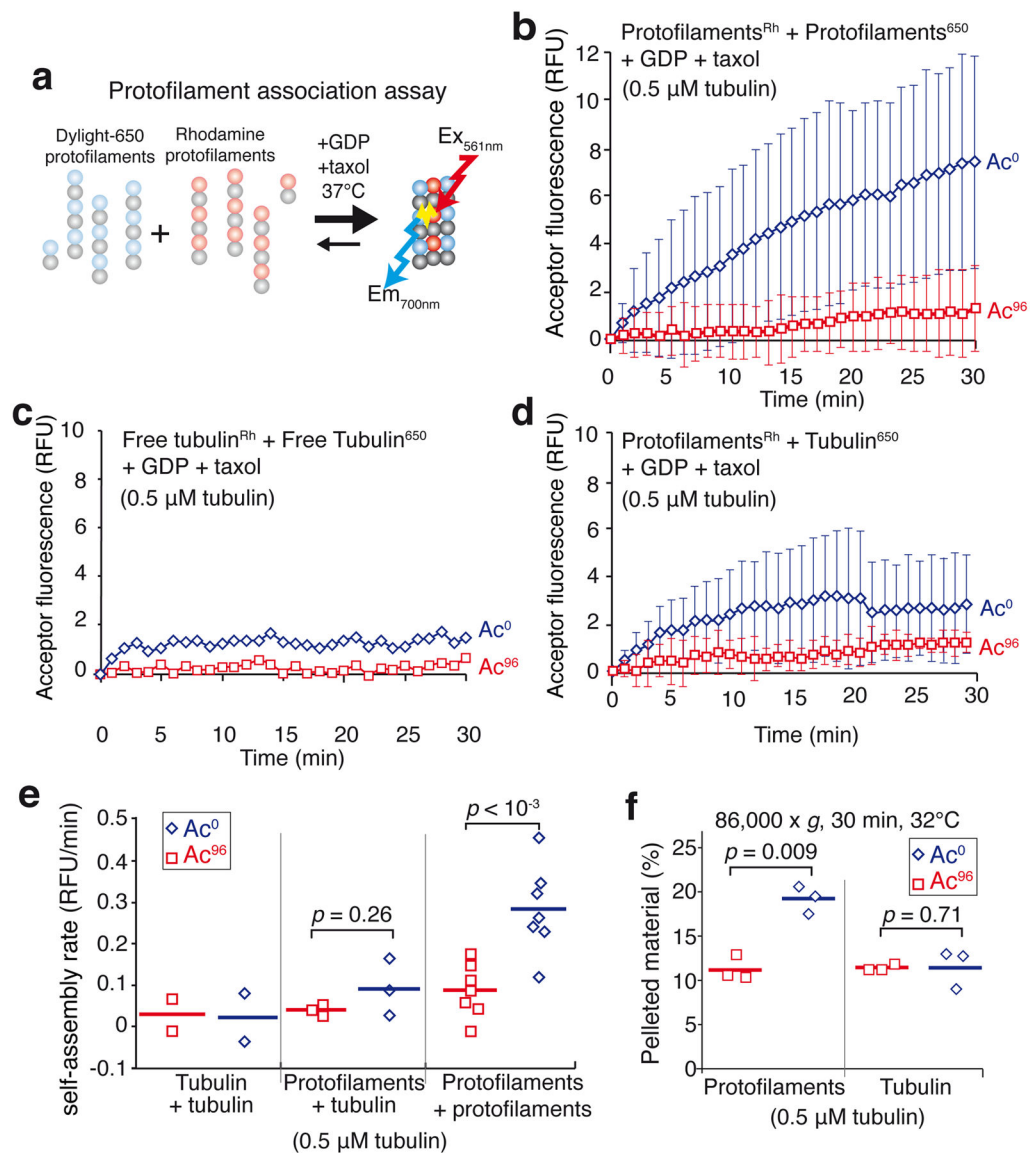


**Figure 3. αK40 acetylation weakens inter-protofilament interactions**

**a**, Diagram of the FRET-based protofilament association assay. Two populations of taxol-stabilized protofilaments were mixed together in the presence of taxol and GDP at 37°C and self-association was followed by monitoring the fluorescence transferred between protofilaments. **b–d**, Self-assembly was assayed in the presence of 1 mM GDP and 0.5 μM taxol at 32°C. FRET was followed in a spectrofluorimeter by exciting rhodamine at 561 nm and measuring DyLight 650 emission at 700 nm. **(b)** Rhodamine-labeled protofilaments were mixed with DyLight 650-labeled protofilaments (each made with a molar ratio of 90% unlabeled tubulin to 10% labeled tubulin). Data points are mean ± SEM. n = 7 independent experiments for both Ac<sup>96</sup> and Ac<sup>0</sup> tubulin. **(c)** Rhodamine- and DyLight 650-labeled tubulin stocks were mixed with unlabeled tubulin so that 10% of the tubulin was rhodamine-labeled and 10% DyLight 650-labeled. Data points are mean of n = 2 experiments for both Ac<sup>96</sup> and Ac<sup>0</sup> tubulin. **(d)** Protofilaments (molar ratio of 90% unlabeled tubulin to 10%

rhodamine-labeled tubulin) were mixed with free tubulin (molar ratio of 95% unlabeled tubulin to 5% DyLight 650-labeled tubulin) to mimic the free tubulin left in solution after protofilament assembly. Data points are mean  $\pm$  SEM. n = 3 independent experiments for both Ac<sup>96</sup> and Ac<sup>0</sup> tubulin. **e**, Dot plot of the self-assembly rates for free tubulin, free tubulin with protofilaments or protofilaments incubated in the presence of 1 mM GDP and 0.5  $\mu$ M taxol at 32°C. The bar denotes the mean. Total tubulin concentration was 0.5  $\mu$ M. The *p*-values of the two-tailed unpaired Student's *t*-tests are indicated. **f**, Dot plot of the amount of tubulin pelleted at 86,000  $\times g_{ave}$  for 30 min at 32°C as a result of the association amongst Ac<sup>0</sup> or Ac<sup>96</sup> protofilaments (n=3 independent experiments). The bar denotes the mean. The *p*-values of the two-tailed unpaired Student's *t*-tests are indicated. Source data for 3c and 3d can be found in Supplementary Table 1.

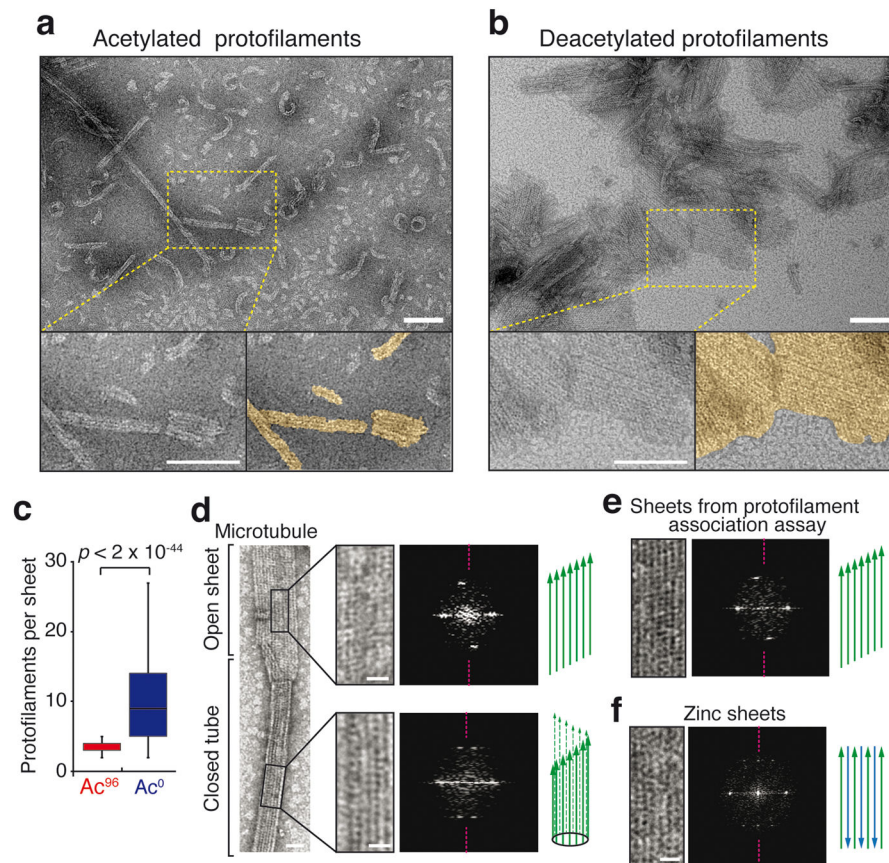


**Figure 4. The protofilament interaction assay produces parallel sheets**

**a,b**, EM micrographs of the protofilaments interaction assays (images are representative of 2 independent experiments). Protofilaments were incubated at 32°C for 30 min with 0.5  $\mu$ M taxol and 1 mM GDP, and imaged by negative-stain EM. The few sheets observed with  $Ac^{96}$  protofilaments contained only 2 to 5 protofilaments (**a**), while extended sheets are seen with  $Ac^0$  protofilaments (**b**). Scale bar = 100 nm. Protofilaments sheets are highlighted in gold color in the magnified bottom right panel of (**a**) and (**b**). Scale bar: 100 nm. **c**, Box plots of the width of sheets (expressed in contiguous protofilament numbers) formed by the association of  $Ac^0$  or  $Ac^{96}$  protofilaments.  $n = 361$   $Ac^{96}$  protofilaments and  $n = 382$   $Ac^0$  protofilaments (pooled from 2 independent experiments). The box represents the 25<sup>th</sup>-75<sup>th</sup> percentile, whiskers indicate 1.5 times the range, bar in the middle is the median **d-f**, Negative stain EM images and associated diffraction patterns; magenta dashed lines indicate the meridian of the diffraction pattern. **d**, The closed microtubule lattice and its diffraction pattern is shown in the bottom right panels while the open sheet and its diffraction patterns is shown on the top right panels. **e**, Protofilament sheet and its diffraction patterns from the protofilament self-assembly assay. **f**, Antiparallel protofilament sheet assembled in presence of zinc. Scale bars: 25 nm (full size images), 10 nm (magnified insets). Diagrams illustrate the known and deduced protofilaments organization. The experiments presented in **d** and **f** were performed once, and the experiment in **e** twice.

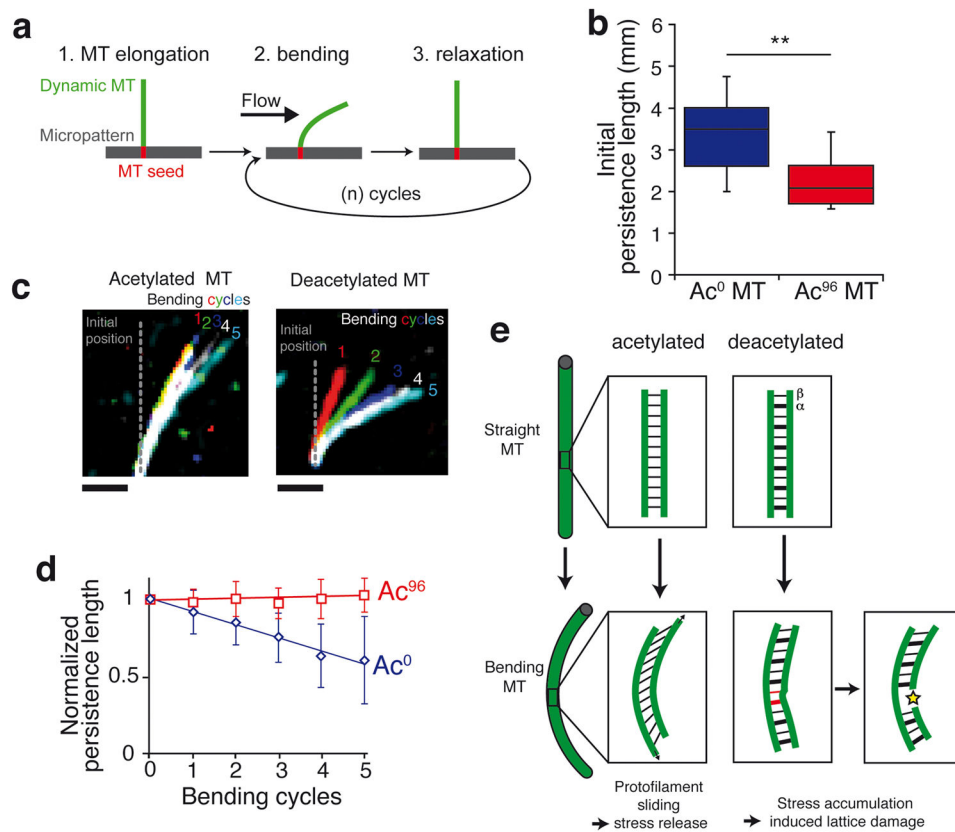


**Figure 5. Acetylation at  $\alpha$ K40 protects microtubules against stress-induced material fatigue**

**a**, Diagram representing the experimental setup used to measure microtubule flexibility and material fatigue. Microtubules were elongated from GMPCPP seeds grafted onto micropatterns, bent using a perpendicular flow for 10 s and then allowed to relax for 10 s. The microtubules are kept dynamic during the experiment by maintaining tubulin concentration at 14  $\mu$ M in the flowing solution. **b**, Microtubule persistence lengths measured during the first bending cycle. \*\* denotes a  $p$ -value of the two-tailed unpaired Student's  $t$ -test  $< 0.01$ ,  $n = 11$   $\text{Ac}^{96}$  microtubules and  $n = 17$   $\text{Ac}^0$  microtubules. The box represents the 25<sup>th</sup>–75<sup>th</sup> percentile, whiskers indicate 1.5 times the range, bar in the middle is the median. **c**, Pseudocolor images of a single representative microtubule at the end of each bending cycle. Scale bar = 5  $\mu$ m. **d**, Plot showing the evolution of persistence length over successive bending cycles. Microtubule persistence lengths were normalized to their initial values (the non-normalized data are shown in Supplementary Figure 5c and d). Data points are mean  $\pm$  SD,  $n = 11$   $\text{Ac}^{96}$  microtubules and  $n = 17$   $\text{Ac}^0$  microtubules. **e**, Model accounting for the increased flexibility and mechanical stability of acetylated microtubules due to decreased inter-protofilament interactions.